RESEARCH

Dynamic characteristics and test research of multibody system considering uneven wear clearances

Shun Gao · Shouwen Fan · Xining Song · Wenjuan Wang

Abstract The wear of rotating pair is a significant factor for the failure of mechanical systems. Currently, some scholars have undertaken investigations on wear clearance, but these works often concentrate on basic systems with even wear clearance, while investigations on multibody systems with uneven wear clearances remains scarce. In addition, the research on wear clearance often focuses on theoretical exploration and computer simulation, while the test research is relatively few. Therefore, a modeling method for 9-bar mechanism with multiple uneven wear clearances is derived by using the Archard model and Lagrange method, the effects of wear times and initial clearance values on dynamic characteristics and nonlinear dynamics of mechanism considering uneven wear clearances are investigated. The test bed of 9-bar mechanism considering clearances is designed and the validity of the theoretical model has been confirmed through a comparison between the collected test data and theoretical data. This paper supplies theory for accurately predicting the dynamic characteristics of multibody system containing uneven wear clearances, and provides proof for identifying and repairing the design defects of mechanism.

Keywords 9-Bar mechanism · Wear clearances · Dynamic characteristics · Nonlinear dynamics · Test research

S. Gao · S. Fan (✉)
School of Mechanical and Electronic Engineering,
University of Electronic Science and Technology of
China-Qingshuihe Campus, Chengdu 611731,
Sichuan, China
e-mail: shouwenfan@263.net

X. Song
School of Mechanical and Electrical Engineering,
Weifang Vocational College, Weifang 262737,
Shandong, China

W. Wang
China Mobile Group Shandong Co., Ltd, Jinan 250000,
Shandong, China

1 Introduction

Mechanisms that utilize rotating pairs as connection methods commonly exist in mechanical systems, such as multi-link press mechanism, multi-DOF manipulator and automobile steering mechanism [1–3]. The ideal rotating pair is difficult to achieve owing to the influence of machining and assembly tolerance, so clearance is inescapable in practical engineering. The clearance will cause the mechanism to operate unsteadily, resulting in the actual operational path of mechanism diverging from the intended path and reducing the motion accuracy of mechanism. Additionally, collisions may occur at clearance during mechanism operation, leading to accelerated wear of components in the rotating pair. Increased wear can generate greater contact force, significantly affecting

the system's working life. Therefore, the research on mechanism considering wear clearances has significant theoretical and practical values.

To establish a reasonable model to characterize contact force of clearance is a critical issue. Earles et al. [4] initially proposed the massless rod model, although the model offers simplified solutions, it overlooks the elastic deformation and separation time occurring during the contact of motion pairs, thus failing to accurately reflect the actual motion state of clearance. Dubowsky et al. [5, 6] Introduced the "contact-separation" model, which considers the contact and separation states of clearance and can easily obtain steady-state solutions. However, because it does not consider parameters such as friction coefficient, stiffness, and damping, it also cannot truly reflect the characteristics of clearance. Miedema et al. [7] proposed the "contact-separation-collision" model, which provides a relatively comprehensive description of the motion state of clearance, yet it is challenging to directly obtain contact force. Soong et al. [8] introduced the transition process into Miedema's model by conducting experiments and analysis on crank-slider mechanism with clearance, making it more aligned with the actual motion conditions of clearance. Consequently, this model has been widely applied in the clearance modeling of mechanisms.

The models commonly for solving the normal contact force of rotating pair include Kelvin-Voigt model [9], Hertz model [10] and Lankarani-Nikravesh (L-N) model [11, 12]. The damping force calculated by Kelvin Voigt model is sometimes inconsistent with the actual situation. The Hertz model is not considering energy loss of system. Comparing to Hertz model, the L-N model considers the energy loss of system, which is better match the actual situation, so it is widely applied to solve contact force of clearance [13]. In addition, the tangential friction force for clearance is usually characterized by the modified Coulomb model [14, 15] and LuGre model [11, 16].

Building upon the aforementioned clearance models, scholars have probed into the dynamic characteristics of systems containing clearances. Guo et al. [17] carried out a model of piston in crank transmission system with clearance joint, which laid a basis for the analysis of piston group. Ordiz et al. [18] performed a method for estimating the impact of changing clearance of moving pair on fatigue life of machine. This

method had higher efficiency and easier operation. Wu et al. [19] explored a variable stiffness model considering the influence of changing geometric to express contact force of clearance. The finite element analysis showed that this model has good predictive performance. Zhuang et al. [20] built a kinetic model of locking system, investigated the time-varying correlation of wear clearance, and discussed reliability evaluation of locking system. Mukras et al. [21] forecasted the performance of crank-slider system under the effect of wear clearance, and verified the method by test research. Alves et al. [22] evaluated the dynamic of rotating system considering the wear of hydrodynamic bearings, and found that the proposed wear model has high accuracy through comparison with experimental data. Flores [23] developed a method for wear model of crank-slider through Archard model, which had high theoretical significance. Singh et al. [24] put forward the effects of wear and lubrication on mechanical systems, and found that lubricants can provide higher value in non-Newtonian states. Lai et al. [25] developed a model of four-bar system and discussed the impact of wear clearance for moving pairs on dynamics of system, which has certain engineering application value. Although scholars have made remarkable achievements on mechanisms with clearance, these studies are usually focused on crank-slider system or 4-bar system with even clearance, but less on complicated system considering several uneven wear clearances.

Up to now, research on mechanisms with clearances has mostly focused on theoretical exploration and computer simulation, while test research on mechanisms with clearances is relatively rare. Although test research on some basic systems with dry friction clearances is advanced, test research on complicated system containing multiple wear clearances is exceedingly rare. Chen et al. [26] carried out a comprehensive analysis on dynamics of press mechanism that contain wear clearances. However, this theoretical study had not been validated by test research. Jiang et al. [27] predicted the dynamic performance of flexible mechanism that contain mixed clearances. However, the effect of wear on mechanism was not considered in study. Zhu et al. [28] derived a way for analyzing wear clearance containing the impact of contact stiffness. Zhuang et al. [29] derived the kinematic accuracy reliability of mechanisms that contain wear clearances and proposed an analytical

method for calculating kinematic reliability based on MCS, the rationality of theoretical model was verified through experimental research. Li et al. [30] had introduced a wear model and studied dynamic performance of crank-slider that contain several wear clearances, and validated the established model by comparing with other literature. Xiang et al. [31] derived a novel algorithm for estimating wear clearance of mechanism. Erkaya et al. [32] established a test bed that considering clearance of crank-slider system, thereby proved the effectiveness of theoretical model. Akhadkar et al. [33] built a 3D rotational clearance model, and the model's rationality was experimentally examined and validated. To validate the predictive ability of clearance model, Flores et al. [34] set up a test device for crank-slider system containing clearances, and discussed the correlation between simulation results and test results. Erkaya et al. [35] explored the performance of articulated mechanism containing clearance through numerical calculation and experimental research and measured the vibration of mechanism. Zheng et al. [36] carried out a dynamic model for flexible system that contain lubrication clearances and established a multi-link press test platform. The study found that the dynamic characteristics of system using this lubrication clearance model is closer to test results, thereby verifying the model.

In summary, the literatures on dynamic characteristics of complicated mechanism containing several wear clearances are few at present. In addition, test research on mechanisms with wear clearances is also very rare. Therefore, so as to supplement the research in this field, the dynamic model of 9-bar mechanism containing 2 wear clearances is set up, the impact of distinct parameters on dynamic characteristics and nonlinear dynamics is analyzed, and the test bed of 9-bar mechanism is designed. The paper contains following parts: In chapter 2, the clearance model is built and the wear phenomenon is described through Archard model. In chapter 3, the dynamic model containing 2 wear clearances is derived through Lagrange method. In chapter 4, the solution flow of this research is described, the geometric parameters of mechanism and clearance are defined. In chapter 5, the effects of wear times and initial clearance values on wear characteristics of rotating pair are studied, the dynamic characteristics and nonlinear dynamics of mechanism considering uneven wear clearances are investigated. In chapter 6, a 9-bar test bed is designed and the theoretical model is validated.

2 Mathematical model of clearance joint

2.1 Dry friction clearance model

Soong's model is used to build the clearance model [8], which is illustrated in Fig. 1. And the mathematical model of clearance is illustrated in Fig. 2. Here, o_i and o_j denote the center of bearing and shaft, e represents eccentric vector, the direction is from bearing center to shaft center, which can be written as

$$e = r_j^O - r_i^O \tag{1}$$

The unit vector n is expressed by

$$n = \frac{e}{e} \tag{2}$$

where e denotes actual size of eccentric vector.

The embedded depth can be obtained by the eccentric vector and the clearance value. The constant ε is used to represent the clearance value, and $\varepsilon = R_1 - R_2$. So the embedded depth δ is written by

$$\delta = e - \varepsilon \tag{3}$$

The position vector for collision point is written by

$$\begin{cases} r_i^{Q_1} = r_i^O + R_1 n \\ r_j^{Q_2} = r_j^O + R_2 n \end{cases} \tag{4}$$

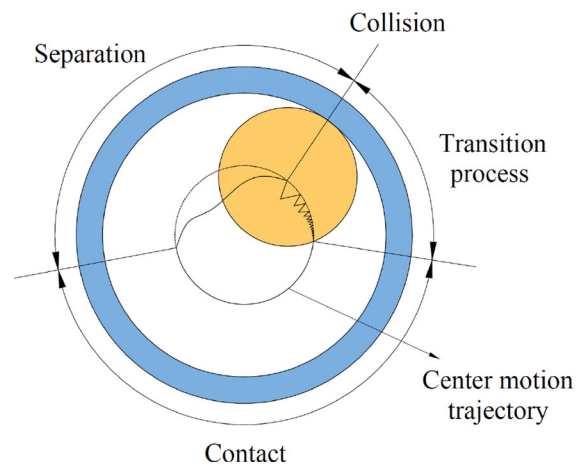where Q_1 and Q_2 denote collision point.
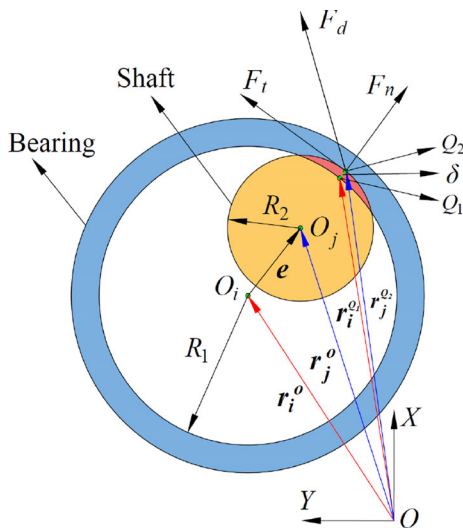

Fig. 1 Soong's model

Fig. 2 Mathematical model of clearance

Formula (4) takes first-order partial derivation of time, the collision velocity is obtained as

$$
\begin{cases}
\dot{\boldsymbol{r}}_i^{Q_1} = \dot{\boldsymbol{r}}_i^{O} + R_1\dot{\boldsymbol{n}} \\
\dot{\boldsymbol{r}}_j^{Q_2} = \dot{\boldsymbol{r}}_j^{O} + R_2\dot{\boldsymbol{n}}
\end{cases}
\tag{5}
$$

Collision velocity can be categorized into v_n and v_t, yielding

$$
\begin{cases}
v_n = (\dot{\boldsymbol{r}}_j^{Q_2} - \dot{\boldsymbol{r}}_i^{Q_1})^{\mathrm{T}}\boldsymbol{n} \\
v_t = (\dot{\boldsymbol{r}}_j^{Q_2} - \dot{\boldsymbol{r}}_i^{Q_1})^{\mathrm{T}}\boldsymbol{t}
\end{cases}
\tag{6}
$$

The L-N model considers the energy loss of system, which is better match the actual situation, which can be expressed as

$$
F_n = F_N + F_f
\tag{7}
$$

where F_N means elastic force which generated by contact deformation of elements of rotating pair, which is expressed as

$$
F_N = K\delta^n
\tag{8}
$$

where F_f means damping force, which is used to represent the energy loss of system, and is expressed as

$$
F_f = D\dot{\delta}
\tag{9}
$$

In formula (8), K represents stiffness coefficient, which is obtained by

$$
K = \frac{4}{3(\delta_1 + \delta_2)}\sqrt{\frac{R_1 R_2}{R_1 + R_2}}
\tag{10}
$$

where $\delta_i = \frac{1-v_i^2}{E_i}(i = 1, 2)$, $v_i(i = 1, 2)$ mean Poisson's ratio of material, $E_i(i = 1, 2)$ mean elastic modulus of material.

In formula (9), $\dot{\delta}$ denotes relative collision velocity, D denotes damping coefficient, which is written by

$$
D = \frac{3K(1 - c_e^2)\delta^n}{4\dot{\delta}_0}
\tag{11}
$$

where c_e means recovery coefficient and $\dot{\delta}_0$ means initial collision speed. n is power exponent of metal surface, and usually taken as $n = 1$ 1.5.

The friction force is resolved via modified Coulomb model, yielding

$$
F_t = -c_f c_d F_n \frac{v_t}{|v_t|}
\tag{12}
$$

where c_f represents friction coefficient. c_d represents correction coefficient, which is

$$
c_d = \begin{cases}
0 & |v_t| \leq v_0 \\
\frac{|v_t| - v_0}{v_m - v_0} & v_0 \leq |v_t| \leq v_m \\
1 & |v_t| \geq v_m
\end{cases}
\tag{13}
$$

where v_0 and v_m denote the speed limit.

From formulas (7) and (12), the contact force F_d is written by

$$
F_d = F_n\boldsymbol{n} + F_t\boldsymbol{t}
\tag{14}
$$

2.2 Wear clearance model

Archard model is widely applied to represent wear characteristic between the elements of rotating pair [26, 29, 30], that is

$$
V = \frac{K_m F_n S}{H}
\tag{15}
$$

where V means wear volume, K_m means wear coefficient, S means sliding distance between the elements of rotating pair during wear, H means surface hardness of softer material, F_n means normal contact force.

Formula (15) is divided by the actual contact area A_α simultaneously, so the Archard model is written by

$$
h = K_n P S
\tag{16}
$$

where $K_n = K_m/H$ denotes linear wear coefficient, $P = F_n/A_\alpha$ denotes contact stress.

The wear schematic diagram of shaft and bearing is illustrated in Fig. 3. Since the contact points of the surfaces of the elements of rotating pair are constantly changing, contact forces and sliding distances are various at various times, formula (17) cannot be directly used for the analysis of the wear characteristics of the rotating pair, so it is changed into a differential form, and the expression is written by

$$\frac{dh}{dS} = K_n P \tag{17}$$

By the finite element method, the sliding distance in time step Δt is ΔS, and it is approximate that the contact force is unchanged in Δt, so wear depth in Δt is written by

$$h_i = K_n P_i \Delta S_i \tag{18}$$

where P_i represents the contact stress. ΔS_i represents the sliding distance increment, and the calculation formula is as follows

$$\Delta S_i = R_1 \Delta \varphi(t_i) \tag{19}$$

$$\Delta \varphi = \varphi_1 - \varphi_2 \tag{20}$$

where φ_1 and φ_2 mean rotation angle of bearing and shaft in time Δt respectively.

In actual operation of mechanism with clearance, multiple contact collisions will occur in a certain section of the elements of rotating pair, so the total wear depth is written by

$$h = \sum h_i \tag{21}$$

Presuming equal wear depths on shaft and bearing, the resulting radii after wear are

$$\begin{cases} R_1^* = R_1 + \dfrac{h}{2} \\ R_2^* = R_2 - \dfrac{h}{2} \end{cases} \tag{22}$$

where R_1^* and R_2^* denote radii of bearing and shaft after wear. After reconstructing the element surface of rotating pair, the second wear of rotating pair can be researched.

## 3 The dynamic model of mechanism with uneven wear clearances

The 9-bar mechanism consists of crank L_1 and L_4, connecting rods L_2, L_3, L_7 and L_8, frame L_5, rocker L_6, and slider S_9, as shown in Fig. 4. Among them, crank L_1 and L_4 are driving link, which are directly driven by the motor and connected to frame L_5 through the rotating pair, the rest of the rods are connected through the rotating pair. The slider is situated at the guide and reciprocates along Y axis driven by the connecting rod L_8. In this paper, clearance A and B are considered simultaneously.

The global coordinate system of mechanism is built by the reference point coordinate method. The mechanism has 8 moving components in total, so generalized coordinates of all components are represented as

$$\boldsymbol{q}_i = \begin{pmatrix} x_i & y_i & \theta_i \end{pmatrix}^{\mathrm{T}} \qquad (i = 1, ..., 9 \qquad i \neq 5) \tag{23}$$

The generalized velocity and acceleration of each component of mechanism are acquired by obtaining the first-order differential and the second-order
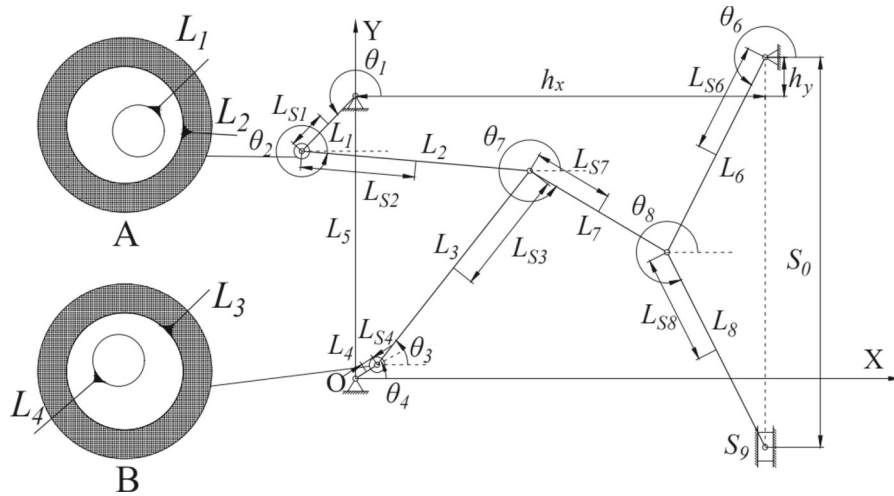
Fig. 3 Wear schematic diagram

(a) Wear of bearing　　　　　　　　　(b) Wear of shaft
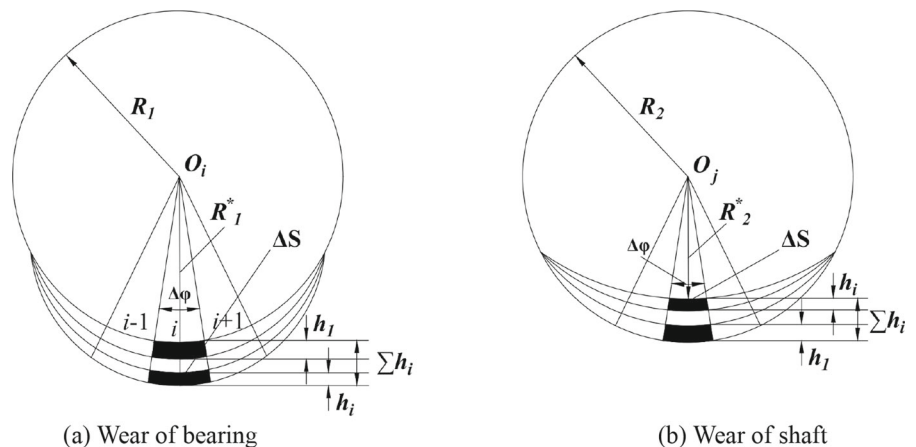
Fig. 4 9-bar mechanism containing wear clearances

differential of time in the global generalized coordinates, which are written by

$$q_i = \begin{pmatrix} \dot{x}_i & \dot{y}_i & \dot{\theta}_i \end{pmatrix}^{\mathrm{T}} \qquad (i = 1, ..., 9 \qquad i \neq 5) \tag{24}$$

$$q_i = \begin{pmatrix} \ddot{x}_i & \ddot{y}_i & \ddot{\theta}_i \end{pmatrix}^{\mathrm{T}} \qquad (i = 1, ..., 9 \qquad i \neq 5) \tag{25}$$

The 9-bar mechanism has 10 rotating pairs and 1 moving pair. The DOF of mechanism is 2, so 2 driving constraint equations are introduced. The constraint of rotating pairs will fail when considering clearances, so the constraint conditions of whole system are written by

Formula (26) obtains the first-order and second-order derivatives of time respectively, the velocity and acceleration constraint equation are obtained as

$$\mathbf{\Phi}_q \dot{q} = -\mathbf{\Phi}_t \equiv v \tag{27}$$

$$\mathbf{\Phi}_q \ddot{q} = -\left(\mathbf{\Phi}_q \dot{q}\right)_q \dot{q} - 2\mathbf{\Phi}_{qt}\dot{q} - \mathbf{\Phi}_{tt} \equiv \gamma \tag{28}$$

where $\dot{q}$ and $\mathbf{\Phi}_q$ denote the generalized velocity vector and Jacobian matrix respectively.

Based on Lagrange method, the dynamics equation is established as

$$\mathbf{M}\ddot{q} + \mathbf{\Phi}_q^{\mathrm{T}}\lambda = g \tag{29}$$

where g denotes generalized force, λ denotes Lagrange multiplier, $\mathbf{M}$ denotes mass matrix.

$$\mathbf{\Phi}(q, t) = \begin{pmatrix} x_1 - L_{s1}\cos\theta_1; & y_1 - L_{s1}\sin\theta_1; & x_4 - L_{s4}\cos\theta_4; & y_4 - L_{s4}\sin\theta_4 + l_5; \\ x_7 - L_{s7}\cos\theta_7 - x_2 - L_{s2}\cos\theta_2; & y_7 - L_{s7}\sin\theta_7 - y_2 - L_{s2}\sin\theta_2 \\ x_7 - L_{s7}\cos\theta_7 - x_3 - L_{s3}\cos\theta_3; & y_7 - L_{s7}\sin\theta_7 - y_3 - L_{s3}\sin\theta_3; \\ x_7 + L_{s7}\cos\theta_7 - x_8 + L_{s8}\cos\theta_8; & y_7 + L_{s7}\sin\theta_7 - y_8 + L_{s8}\sin\theta_8; \\ x_7 + L_{s7}\cos\theta_7 - x_6 - L_{s6}\cos\theta_6; & y_7 + L_{s7}\sin\theta_7 - y_6 - L_{s6}\sin\theta_6; \\ x_6 - L_{s6}\cos\theta_6 - h_x; & y_6 - L_{s6}\sin\theta_6 - h_y; & x_9 - L_{s8}\cos\theta_8 - x_8; \\ y_9 - L_{s8}\sin\theta_8 - y_8; & x_9 - h_x; & \theta_9 - 90°; & \theta_1 - \omega_1 t + 36.84°; \\ & & \theta_4 - \omega_4 t - 24.31° \end{pmatrix} = \mathbf{0} \tag{26}$$

The dynamic equation containing clearances via Baumgarte's algorithm is obtained as [37]

$$\begin{pmatrix} M & \Phi_q^{\mathrm{T}} \\ \Phi_q & 0 \end{pmatrix} \begin{pmatrix} \ddot{q} \\ \lambda \end{pmatrix} = \begin{pmatrix} g \\ \gamma - 2\alpha\dot{\Phi} - \beta^2\Phi \end{pmatrix} \qquad (30)$$

where α and β represent the correction coefficient, and $\dot{\Phi} = d\Phi/dt$.

4 Solution of dynamic equation of mechanism with wear clearances

4.1 Solving steps of dynamic equation

As illustrated in Fig. 5, the specific solving process is:

1. The initial parameters of 9-bar mechanism are defined;
2. Determine if there is a collision between shaft and bearing. If no collision, the dynamic equation is calculated directly. If collision, the contact force is obtained by L-N model and wear depth are calculated through Archard model, the surface of rotating pair is reconstructed by wear depth, and then the dynamic equation containing uneven wear clearances is calculated;
3. The dynamic equation is settled by Runge–Kutta algorithm by MATLAB software, the generalized coordinates and velocity are obtained;
4. Loop the above steps until time runs out.

4.2 Simulation parameters of mechanism

The clearance parameters of rotating pair are gathered in Table 1, and the mechanism's structural parameters are gathered in Table 2. The selection criteria for simulation parameters can refer to literatures [37, 38].

4.3 Assumption of wear conditions

So as to predict the wear of mechanism and increase the calculation efficiency, the assumptions are made as follows

1. The rotating pair's surface is segmented into 1000 distinct regions based on finite element theory, and the wear depth in each wear region of elements of rotating pair is calculated.
2. The wear depth is determined at every 100 operation cycles for mechanism, and the wear depth is multiplied by 2000 to estimate the total wear depth of the rotating pair after 200,000 operation cycles.
3. Assuming that 200 thousand motion cycles are regarded as a wear cycle, the surfaces of the elements of rotating pair in first wear cycle are reconstructed and the dynamic characteristics are researched, which is called first wear. Reconstituting the surfaces of elements of rotating pair in second wear cycle and analyzing dynamic characteristics of mechanism is called second wear.
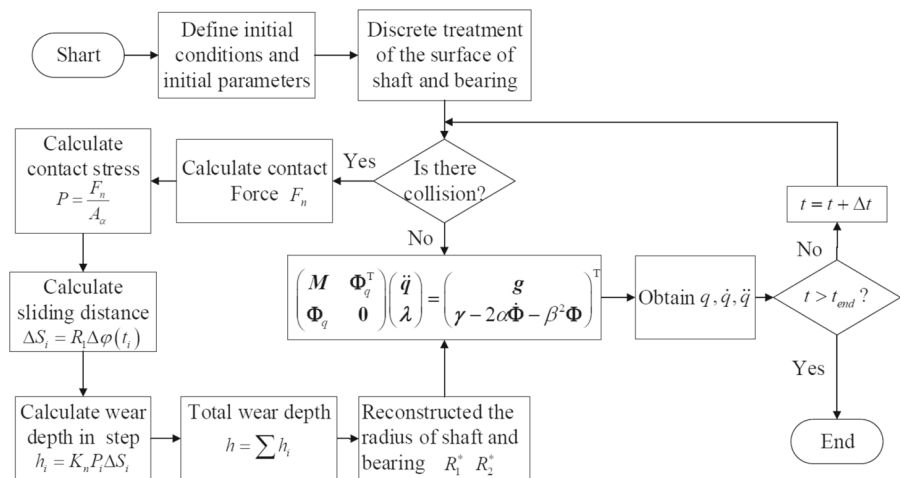

Fig. 5 Flow chart of solution

Table 1 Clearance parameters of rotating pair

Parameter	Values	Parameter	Values
Coefficient of correction α, β	20	Poisson's ratio v_i	0.3
Recovery coefficient c_e	0.9	Integral step (s)	0.0001
Elastic modulus $E_i/(GPa)$	206	Bearing radius $R_1/(m)$	0.015
Friction coefficient c_f	0.1	Surface hardness $H/(Mpa)$	217

Table 2 Mechanism's structural parameters

Member	Values/m	Mass/kg	Moment of inertia/kg m^2
L_1	0.300	0.985	8.390×10^{-3}
L_2	0.893	2.836	1.962×10^{-1}
L_3	0.962	3.051	2.444×10^{-1}
L_4	0.100	0.361	4.773×10^{-4}
L_6	0.850	2.701	1.691×10^{-1}
L_7	0.623	1.993	6.818×10^{-2}
L_8	0.850	2.701	1.691×10^{-1}
S_9	–	4.288	1.004×10^{-1}
L_5	1.100	–	–
h_x	1.600	–	–
h_y	0.150	–	–

5 The dynamic characteristics and nonlinear dynamics of mechanism considering uneven wear clearances

According to the established model and simulation parameters, the dynamic characteristics and nonlinear dynamics of 9-bar mechanism are investigated. And different driving speeds and clearance values are used in different sections to enrich the results.

5.1 The effects of wear times on dynamic characteristics and nonlinear dynamics of mechanism

In this part, the impact of wear times on dynamic characteristics and nonlinear dynamics of mechanism containing uneven wear clearances are researched. The initial clearance value is 0.6 mm, and the driving speeds are $\omega_1 = \omega_4 = -5\pi\mathrm{rad}/s$. The wear depth and the surface of bearing and shaft after wear are illustrated in Figs. 6, 7 and 8.

As illustrated in Fig. 6, the wear areas of clearance A are mainly concentrated in [0°, 110°], [200°, 272°] and [326°, 360°], the largest wear depth of first wear

and second wear are 4.73e−05 m and 1.16e−04 m respectively. The wear areas of clearance B are mainly concentrated in [93°, 162°] and [235°, 338°], and the largest wear depths of first wear and second wear are 1.47e−05 m and 2.67e−04 m respectively. As illustrated in Figs. 7 and 8, the surface of bearing and shaft is uneven after wear. And the second wear has a more pronounced effect on the surface of bearing and shaft than first wear. In addition, The wear depth of clearance B exceeds that of clearance A.

The dynamic characteristics of system considering different wear times are explored. The slider's outputs are illustrated in Figs. 9, 10 and 11, the contact force and the center trajectory are illustrated in Figs. 12 and 13.

As illustrated in Fig. 9, the slider's displacement before and after wear is basically coincide, suggesting that the wear clearances minimally affect the slider's displacement. As illustrated in Fig. 10, the slider's velocity before and after wear is basically coincide, but the velocity curve after wear has obvious sawtooth fluctuations, and the fluctuation of second wear is larger than that of first wear. As illustrated in Fig. 11, the wear clearance exerts significant influence on slider's acceleration. Before wear, after first wear and after second wear, the largest slider's acceleration occurs at 0.011 s, 0.222 s and 0.329 s respectively, and the peak values are 463.2 m/s^2, 2333 m/s^2 and 3231 m/s^2 respectively. The above results indicate that as the increase of the wear times, the fluctuation degree and peak values of slider's outputs will increase.

The contact force before and after wear is illustrated in Fig. 12. It shows that when considering before wear, after first wear and after second wear, the largest contact force of clearance A occur at 0.004 s, 0.004 s and 0.214 s respectively, and the peak values are 2912N, 6602N and 11230N respectively. Meanwhile, the largest contact force of clearance B occur at 0.011 s, 0.214 s and 0.236 s respectively, and the values are 3032N, 11690N and 15340N respectively. The results indicate that the contact force increase
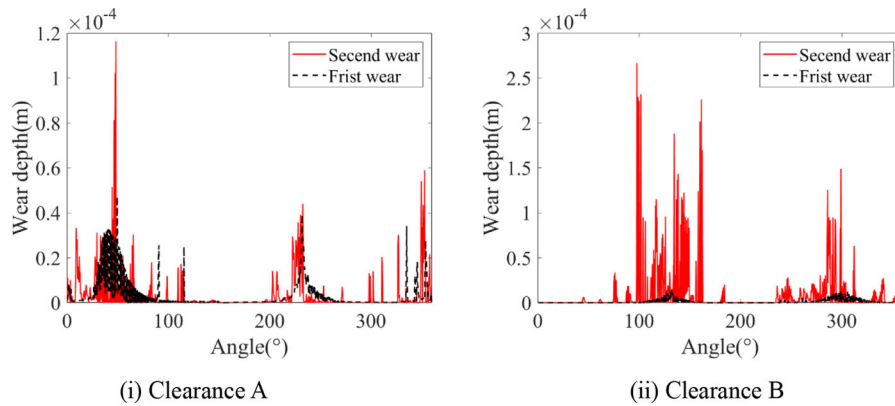
(i) Clearance A   (ii) Clearance B

Fig. 6 Wear depth

Fig. 7 Surface of bearing after wear

(i) Surface of bearing A   (ii) Surface of bearing B

Fig. 8 Surface of shaft after wear

(i) Surface of shaft A   (ii) The surface of shaft B
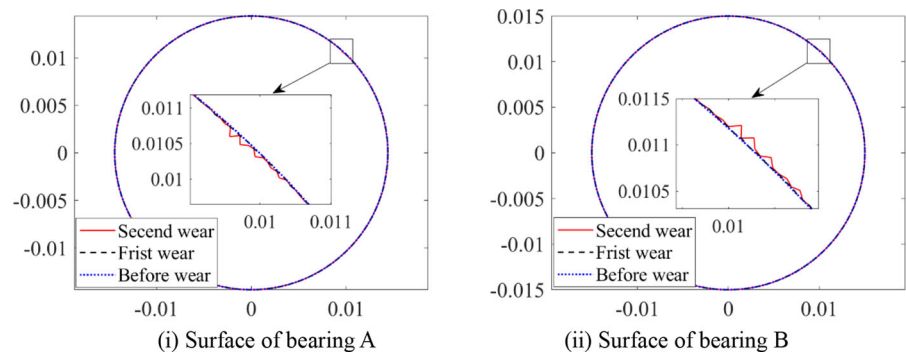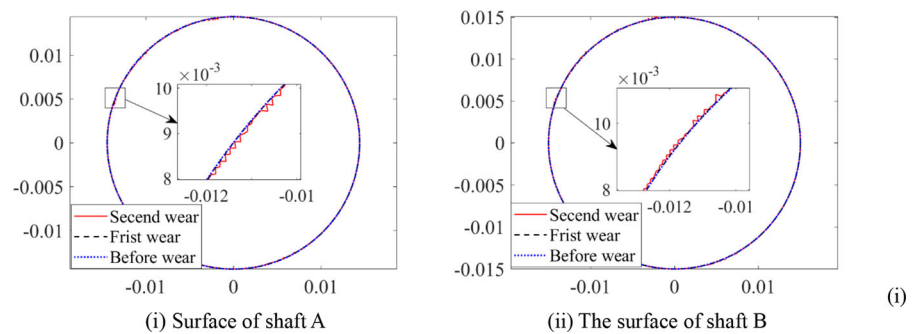
significantly after wear. The center trajectory of shaft is illustrated in Fig. 13, the center trajectory will be more chaotic and the motion range will be larger after second wear. The results prove that the second wear plays a major role on dynamic characteristics of system.

The Poincare diagram can reflect the impact of clearance joint on the performance of system, and can more accurately describe the periodic motion, stability, and chaotic motion of system. The Phase diagram can help determine the stable motion state of the system within different parameter ranges. The Poincare diagram and Phase diagram of clearance A and clearance B are illustrated in Figs.14, 15, 16 and 17.

As illustrated in Figs.14 and 15, when considering before wear, the mapping points of clearances A and B in Poincare diagram in X and Y directions are relatively concentrated, indicating that clearances A and B are in periodic motion. When considering first wear and second wear, the scattering of mapping
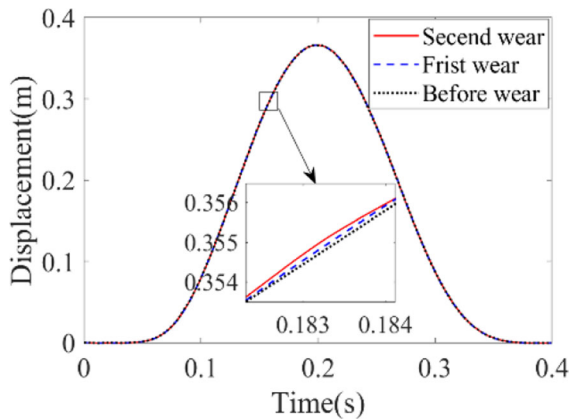
Fig. 9 Displacement
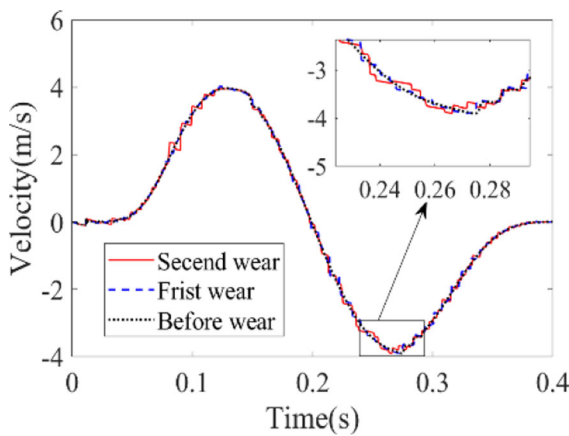
Fig. 10 Velocity
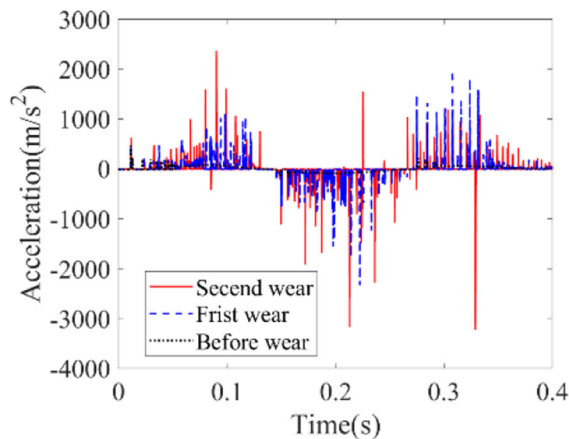
Fig. 11 Acceleration

points in the Poincare diagram increases, suggesting that clearances A and B exhibit chaotic motion.

The Phase diagram of clearances A and B are illustrated in Figs. 16 and 17. When considering before wear, first wear and second wear, the trajectory range of Phase diagram in X and Y directions is constantly increasing, which indicates that the movement of mechanism becomes more unstable after wear.

5.2 The effects of initial clearance values on dynamic characteristics and nonlinear dynamics of mechanism

In this part, the effects of initial clearance values on dynamic characteristics and nonlinear dynamics of mechanism are researched. Take the driving speeds as $\omega_1 = \omega_4 = -6\pi\text{rad/s}$ and take the initial clearance values as 0.1 mm, 0.3 mm and 0.45 mm respectively. The wear depth at clearance and the surface of bearing and shaft after wear are illustrated in Figs. 18, 19, 20 and 21.

As illustrated in Fig. 18, the wear depth and the wear range of clearance will enlarge with the increase of initial clearance values, and the wear depth of clearance B is more severe. The wear areas of clearance A are mainly concentrated in [0°, 150°] and [216°, 270°], when the clearance values are 0.1 mm, 0.3 mm and 0.45 mm respectively, the largest wear depths are 1.91e-06 m, 3.96e-06 m and 1.22e-05 m respectively. The wear areas of clearance B are mainly concentrated in [80°, 159°] and [244°, 360°], when the clearance values are 0.1 mm, 0.3 mm and 0.45 mm respectively, the largest wear depths are 3.90e−06 m, 1.15e−05 m and 2.58e−05 m respectively. The above results indicate that the wear phenomenon can be reduced by appropriately reducing the clearance values. As illustrated in Figs. 19, 20 and 21, the wear degrees of surface of clearance are distinct when the initial clearance values are distinct, and the larger the initial clearance values, the greater the wear degree of clearance. This phenomenon arises from the fact that when the clearance increases, the movement of the shaft and bearing becomes more unstable, leading to greater contact force between
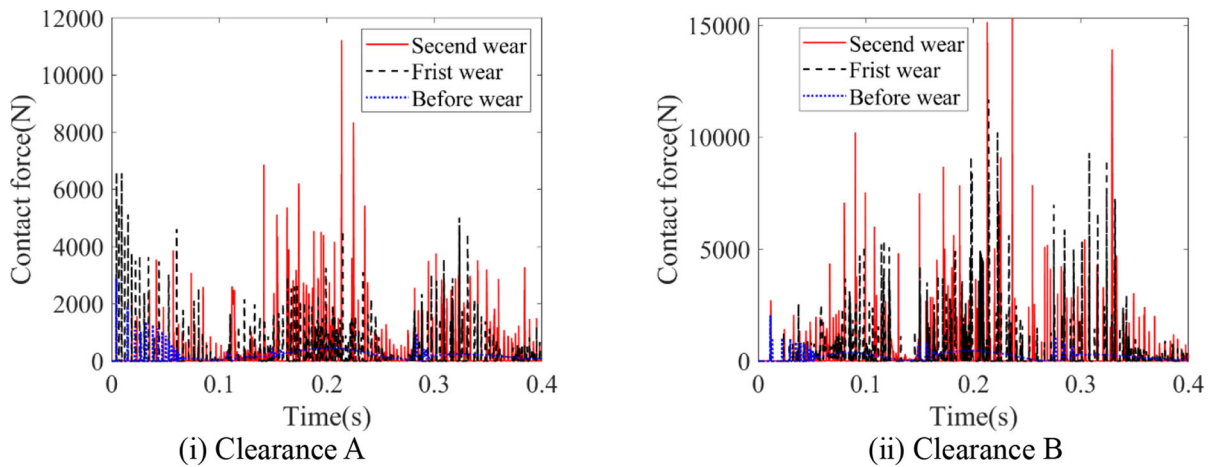
Fig. 12 Contact force of clearance
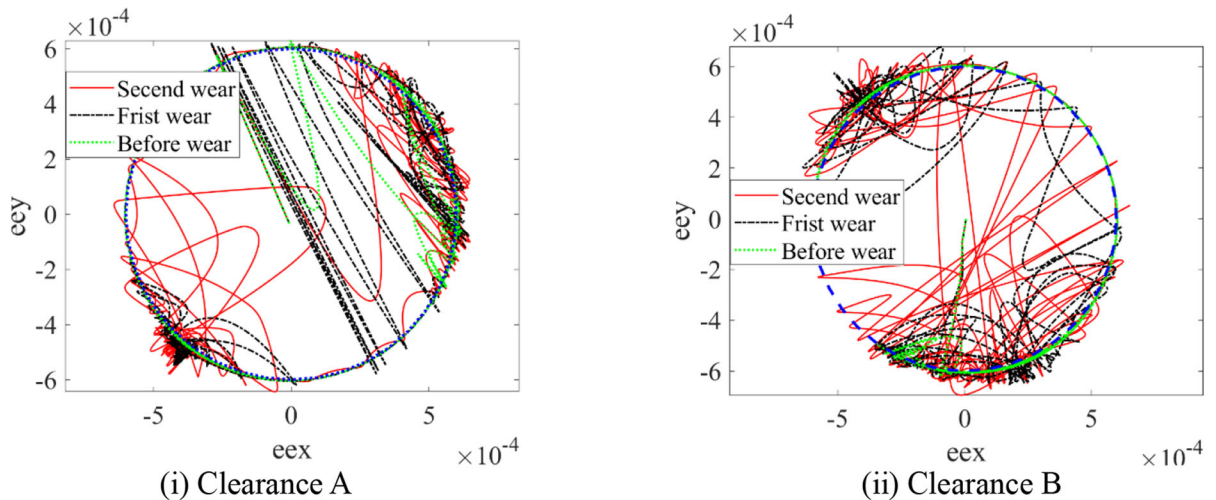
Fig. 13 Center trajectory of shaft

them, thereby accelerating the wear of the contacting surfaces in the motion pair.

The dynamic characteristics of mechanism considering different initial clearance values are analyzed. The slider's outputs are illustrated in Figs. 22, 23 and 24, the contact force and the center trajectory are illustrated in Figs. 25, 26, 27 and 28.

As illustrated in Fig. 22, when the initial clearance values are 0.1 mm, 0.3 mm and 0.45 mm respectively, the slider's displacement before and after wear is basically the same, which indicates that the wear clearance has less impact on displacement. As illustrated in Fig. 23, the slider's velocity after wear appears obvious fluctuations and the larger the

clearance value, the greater the impact on slider's velocity. As illustrated in Fig. 24, the slider's acceleration vibrates violently after wear, and these vibrations exhibit a higher frequency and greater amplitude when the initial clearance value is set at a larger value. When the initial clearance value is 0.1 mm, the largest slider's acceleration before and after wear occur at 0.005 s and 0.041 s respectively, and the peak values are 155.3 m/s^2 and 308.4 m/s^2 respectively. When the initial clearance value is 0.3 mm, the largest slider's acceleration before and after wear occur at 0.049 s and 0.191 s respectively, and the peak values are 334.4 m/s^2 and 1145 m/s^2 respectively. When the initial clearance value is 0.45 mm, the largest slider's

(i) X-direction

(ii) Y-direction

Fig. 14 Poincare diagram of clearance A

(i) X-direction

(ii) Y-direction
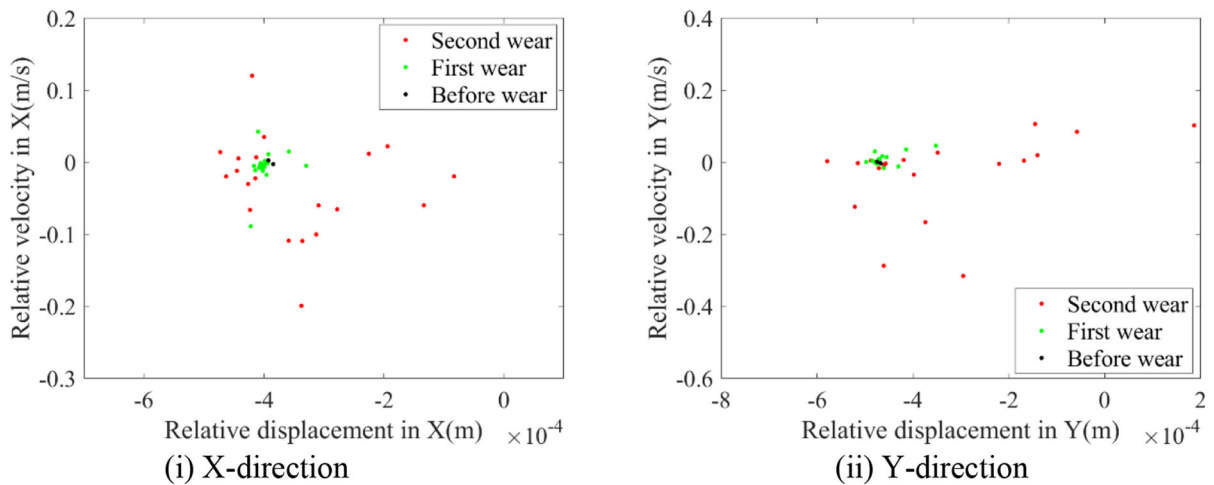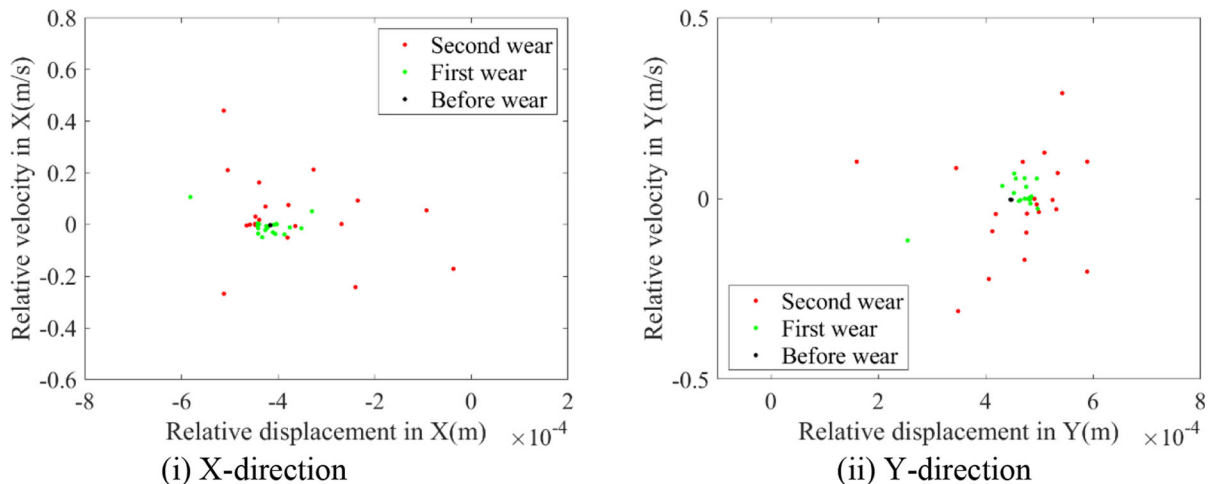
Fig. 15 Poincare diagram of clearance B

acceleration before and after wear occur at 0.049 s and 0.191 s respectively, and the peak values are 597.7 m/s² and 3289 m/s² respectively. In summary, the wear clearance has the least impact on slider's displacement and has the largest impact on slider's acceleration.

When considering different initial clearance values, the contact force before and after wear at clearance are illustrated in Figs. 25 and 26. The table offers a clearer visualization of how contact force varies with different initial clearance values, as demonstrated in Table 3.

The results in Table 3 show that the contact force at clearance increases greatly after wear, and the larger the initial clearance value, the larger the contact force at clearance.

The center trajectory of shaft with different initial clearance values are illustrated in Figs. 27 and 28. The motion of the center trajectory of clearance is more chaotic and has a larger range after wear. And with the increase of initial clearance values, the motion range of the center trajectory of clearance is significantly increased and more disordered.

The nonlinear dynamics of uneven wear clearances is analyzed under different initial clearance values. The
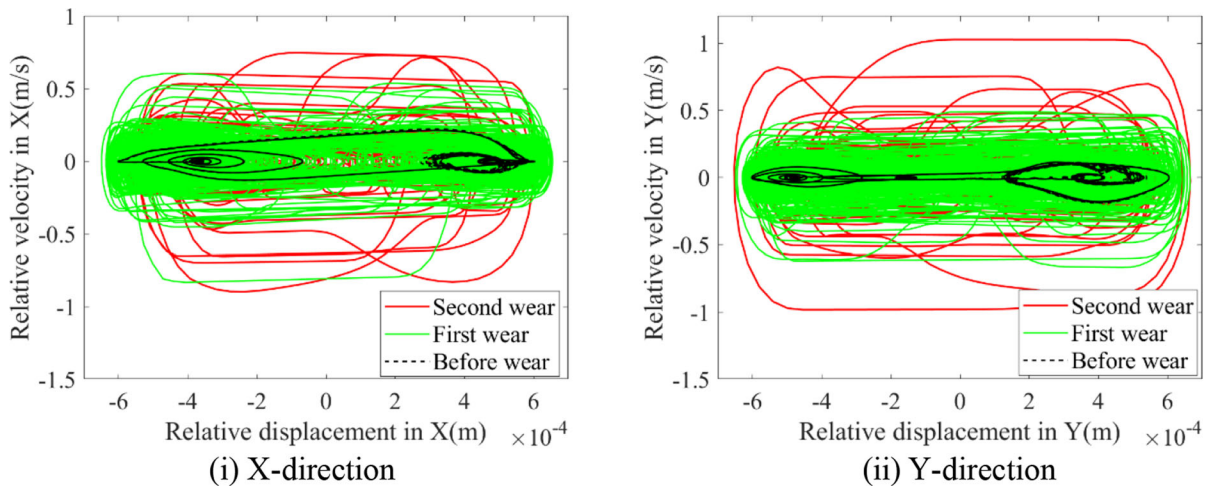
Fig. 16 Phase diagram of clearance A
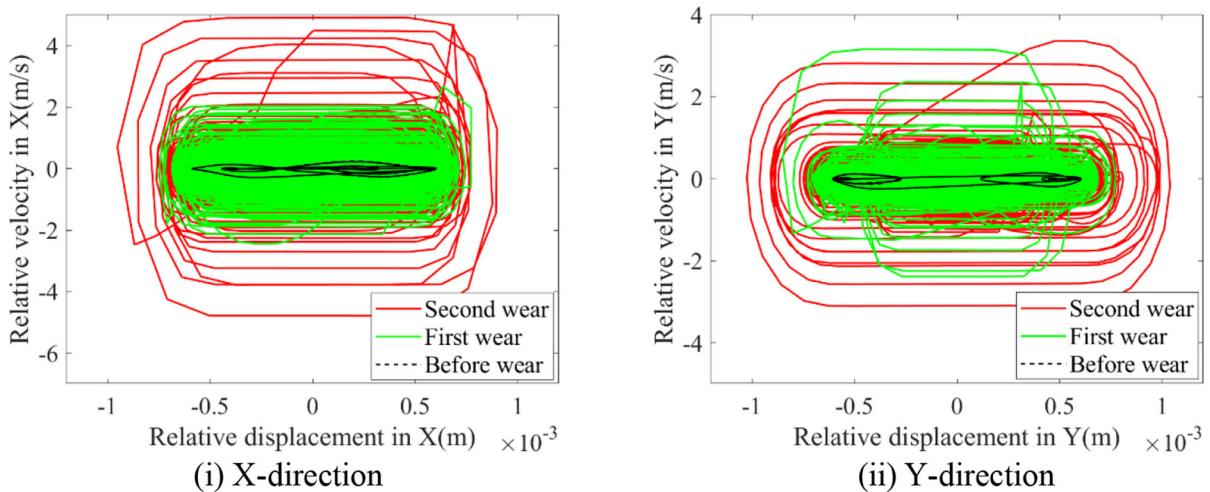
Fig. 17 Phase diagram of clearance B

Poincare diagram and Phase diagram of clearance A and clearance B are illustrated in Figs. 29, 30, 31 and 32.

As illustrated in Figs. 29 and 30, the mapping points of clearances A and B in X and Y directions become more dispersed with the increase of initial clearance values, which indicates that clearances A and B are transforming from periodic motion to chaotic motion after wear. The Phase diagram of clearances A and B are illustrated in Figs. 31 and 32. The trajectory range of Phase diagram in X and Y directions is constantly increasing as the initial clearance values increase.

6 Test research

6.1 Construction of test bed

To validate the accuracy of the clearance model and wear model used in this study, a 9-bar test bed is built, as illustrated in Fig. 33. The test bed is designed by 9-bar mechanism, which includes the structural system, the speed control system, and the data acquisition system. The frame and each rod are made of 6061 aluminum alloy material, and the considers clearance at rotating pair A and B. The servo stepper motor is

Fig. 18 Wear depth

(i) Clearance A

(ii) Clearance B

Fig. 19 Surface of bearing after wear

(i) The surface of bearing A

(ii) The surface of bearing B

(i) 0.1mm

(ii) 0.3mm

(iii) 0.45mm
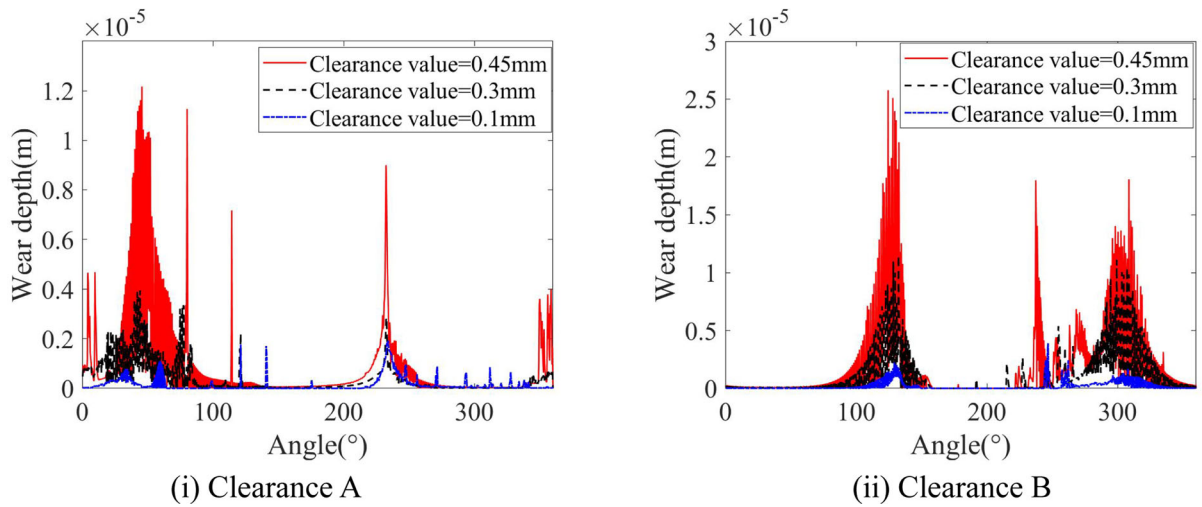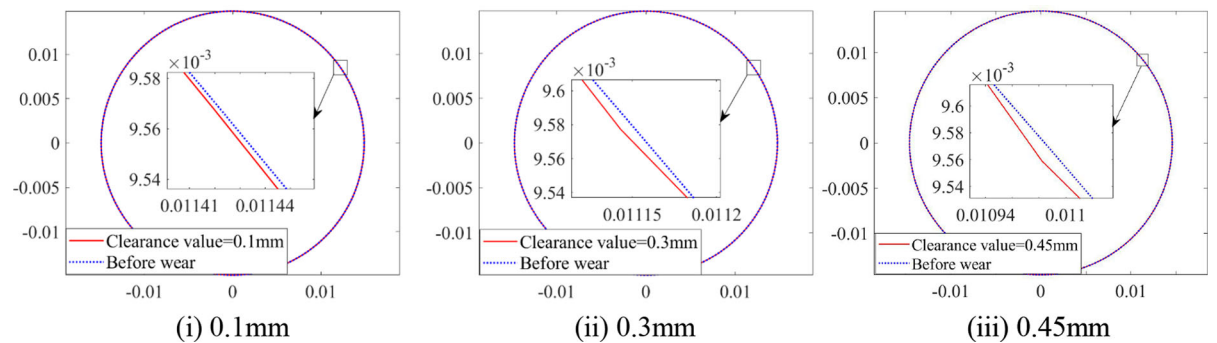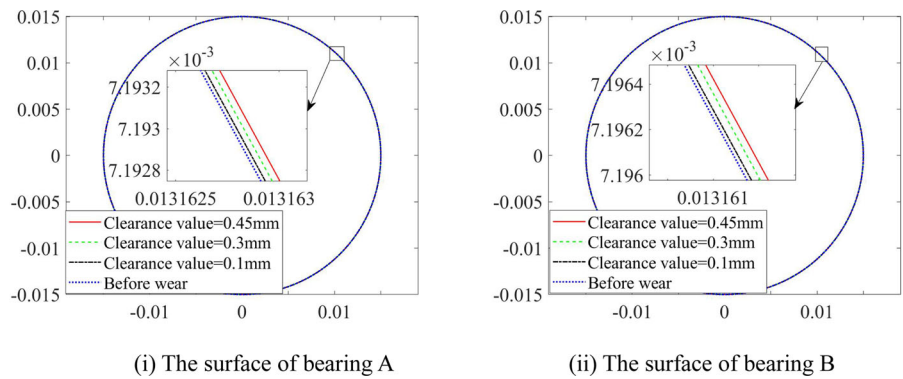
Fig. 20 Surface of shaft A

installed under the support plate to provide the original drive for test bed. The motor is connected to the crank through a coupling, and the rotation of the crank drives each rod to move in the plane, the slider is driven to perform reciprocating linear motion in the guide rail. The acceleration sensor is directly connected to the end of slider to test the acceleration signal of slider. The data acquisition card is used to collect the signal
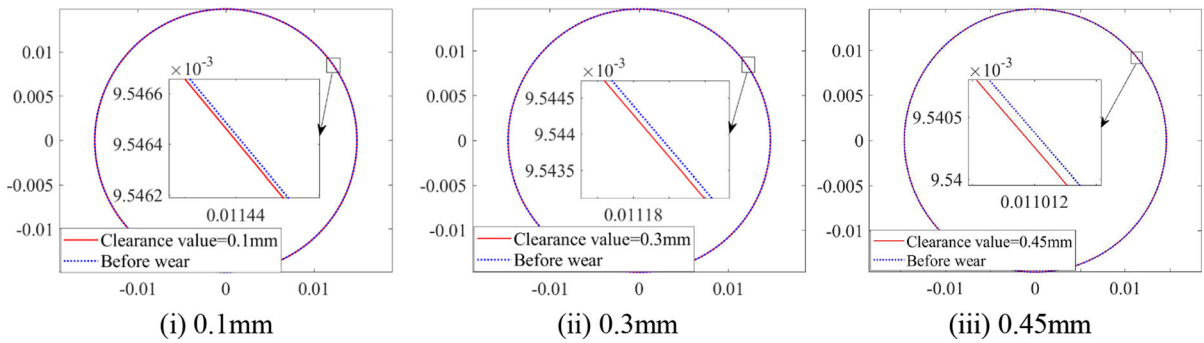
Fig. 21 Surface of shaft B
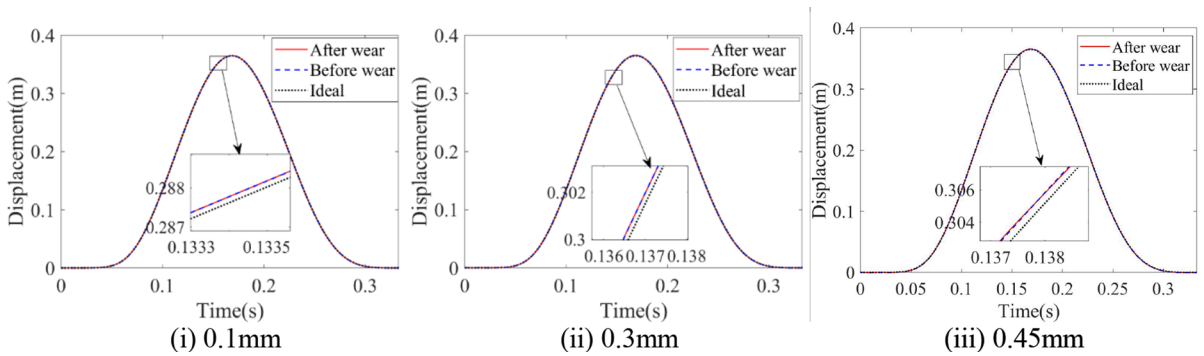
Fig. 22 Displacement
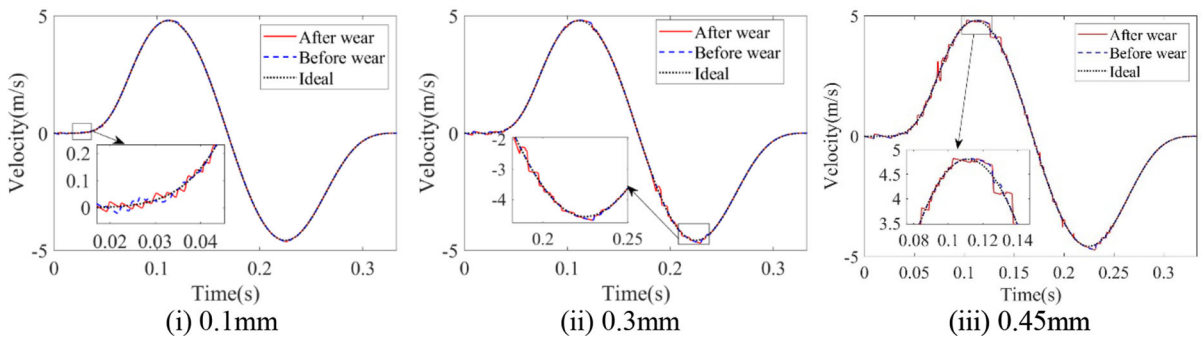
Fig. 23 Velocity

of acceleration sensor and transmit it to PC, and the test results are handled and stored through LabVIEW software.

In order to observe the test effects and highlight the effects of clearances on the performance of mechanism, the clearance values processed in this test may be higher than actual engineering practice. In this test, consider the clearance A and clearance B in Fig. 33. The rest of rotating pairs use interference fit to achieve

an ideal rotating pair. The different clearance values are constructed by machining shafts with different diameters, as shown in Figs.34 and 35.

During the test process, many factors may cause errors of test results, reducing the accuracy of the results. Therefore, when assembling the test bed, it is necessary to note the following issues:
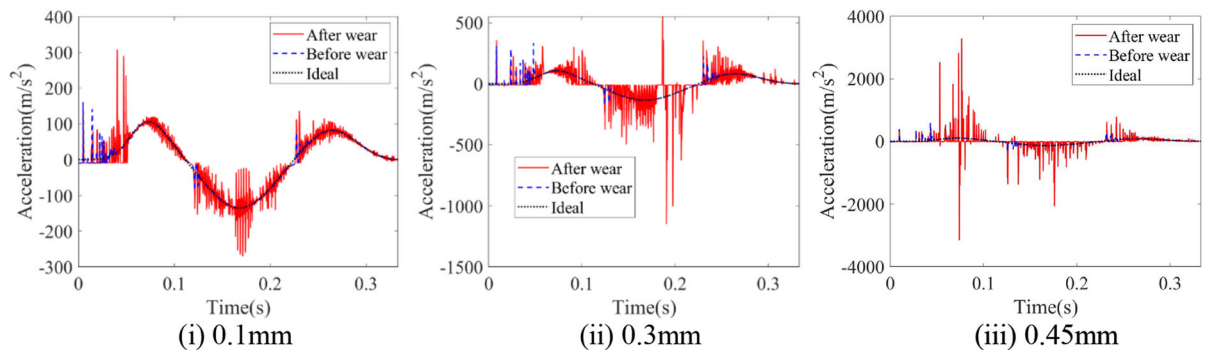
Fig. 24 Acceleration
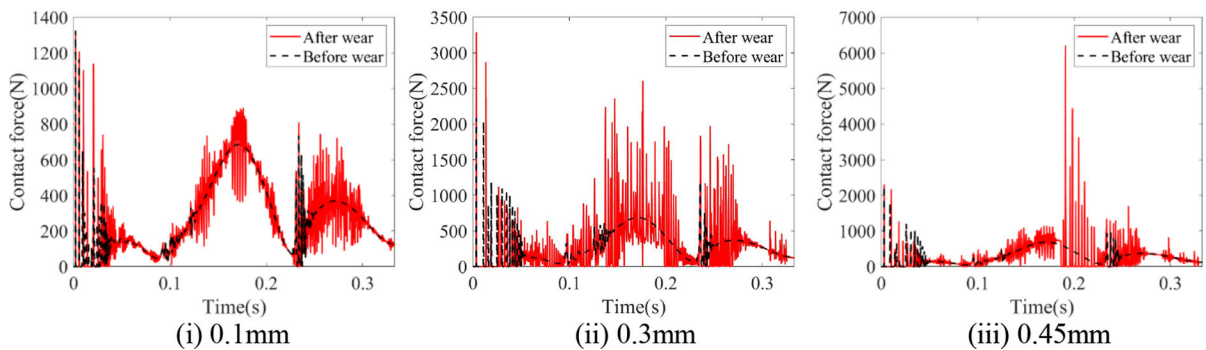
Fig. 25 Contact force of clearance A
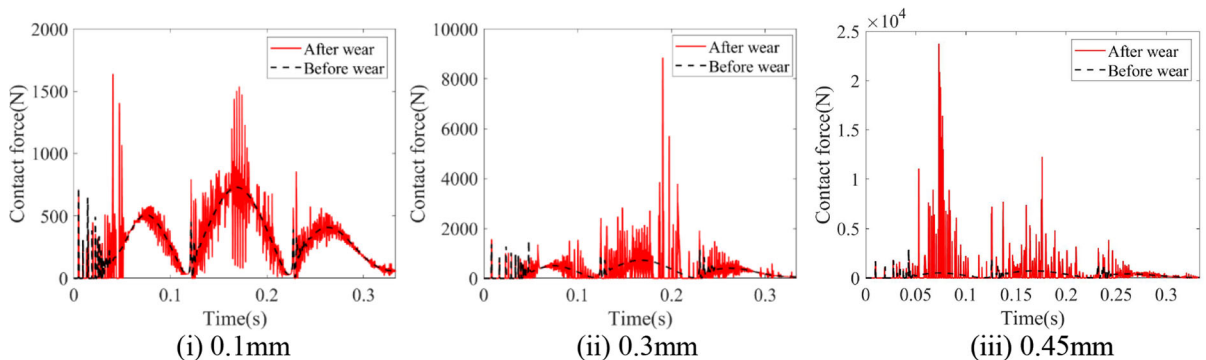
Fig. 26 Contact force of clearance B

1. During the processing of each component of mechanism, try to improve the processing accuracy to ensure the accuracy of each component;
2. Pay attention to the vibration isolation and damping to reduce the impact of the vibration generated by test bed on test results;
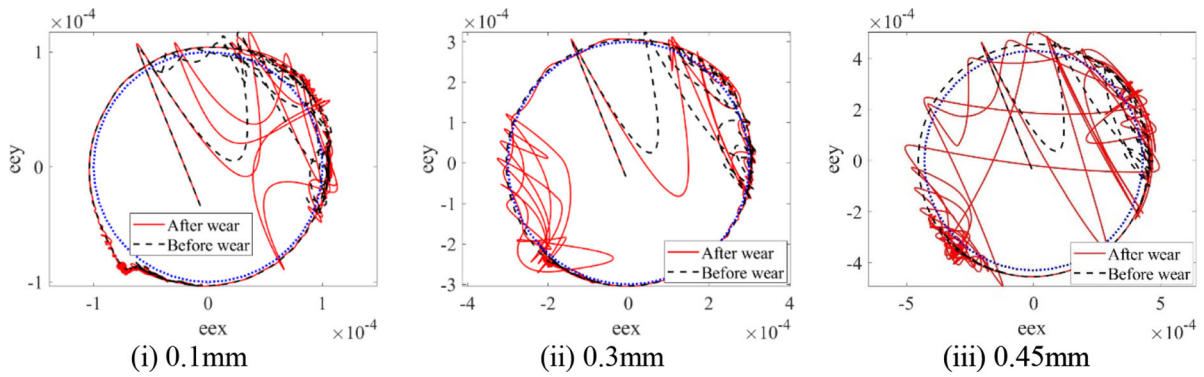3. Accurately locate the initial position of each component to prevent the impact of accumulated errors on mechanism.

Fig. 27 Center trajectory of clearance A
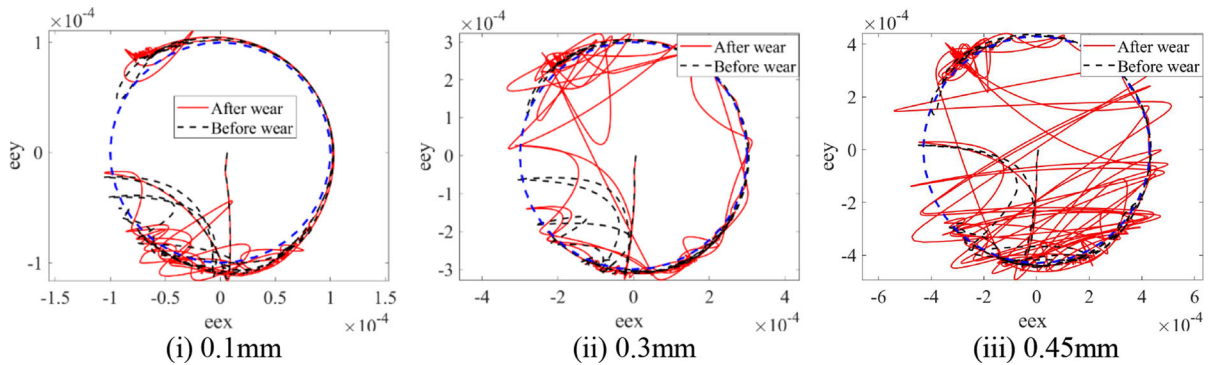
Fig. 28 Center trajectory of clearance B

Table 3 The maximum contact force considering different initial clearance values

Clearance Value	0.1 mm		0.3 mm		0.45 mm	
	Before wear	After wear	Before wear	After wear	Before wear	After wear
Clearance A	1322N	1327N	2086N	3289N	2269N	6214N
Clearance B	724.4N	1639N	1507N	8849N	2928N	23750N

6.2 The effects of initial clearances on dynamic characteristics of test bed

Take the driving speeds as $\omega_1 = 2\pi \text{rad/s}$, $\omega_2 = -2\pi \text{rad/s}$. Randomly intercept the test results for five motion cycles when considering different clearances, as illustrated in Fig. 36. Compare the test data with the theoretical data, as illustrated in Fig. 37.

As illustrated in Fig. 36, when the clearance values are 0.6 mm, the vibration amplitude and peak values of slider's acceleration are significantly larger, which means that the larger the clearance values, the greater the impact on slider's acceleration. As illustrated in Fig. 37, before wear, the theoretical results of slider's acceleration basically agree with the test results in trend, only with a slight difference in peak values. The possible reason is that the vibration generated during the operation of system may have a certain impact on test data. In summary, the theoretical data are basically consistent with the test data, thereby verifying the correctness of clearance model.
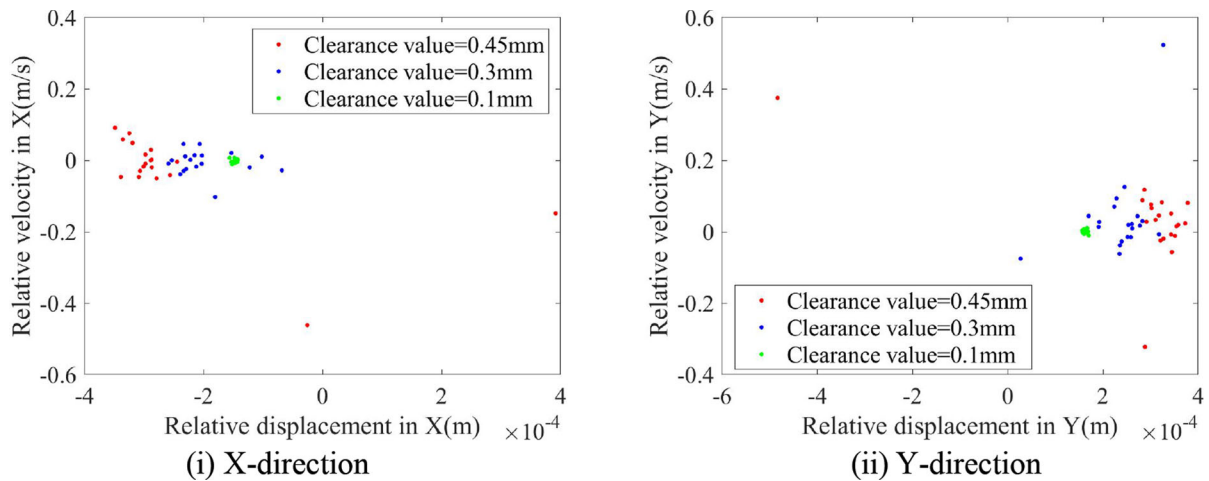
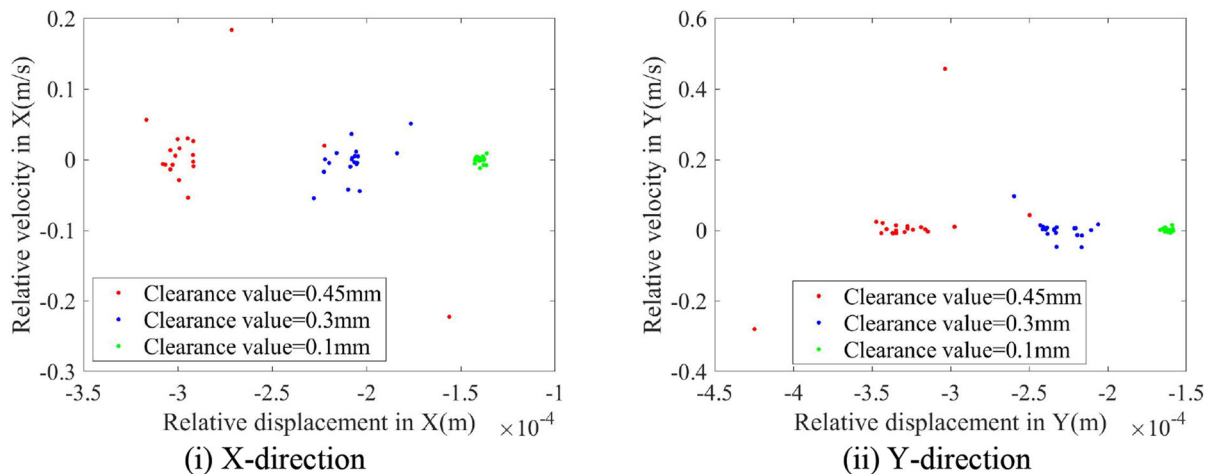**Fig. 29** Poincare diagram of clearance A

Fig. 30 Poincare diagram of clearance B

6.3 The effects of wear clearances on dynamic characteristics of test bed

Take the driving speeds as $\omega_1 = 2\pi\,\mathrm{rad/s}$, $\omega_2 = -2\pi\,\mathrm{rad/s}$, and take the initial clearance value as 0.3 mm. Collect the test results when the crank rotates 200 thousand motion cycles (that is first wear) and when the crank rotates 400 thousand motion cycles (that is second wear). Randomly intercept the test results for five motion cycles when considering different wear times, as illustrated in Fig. 38. Compare the test data with the theoretical data, as illustrated in Fig. 39.

As illustrated in Fig. 36, when the crank rotates 400 thousand motion cycles, the vibration amplitude and peak value of slider's acceleration are significant. As illustrated in Fig. 38, after first wear and second wear, the theoretical and test data for slider's performance exhibit a closely aligned trend, thereby validating the accuracy of the wear clearance model.

7 Conclusion

A dynamic model of 9-bar mechanism considering multiple uneven wear clearances is derived in this study, the dynamic characteristics and nonlinear
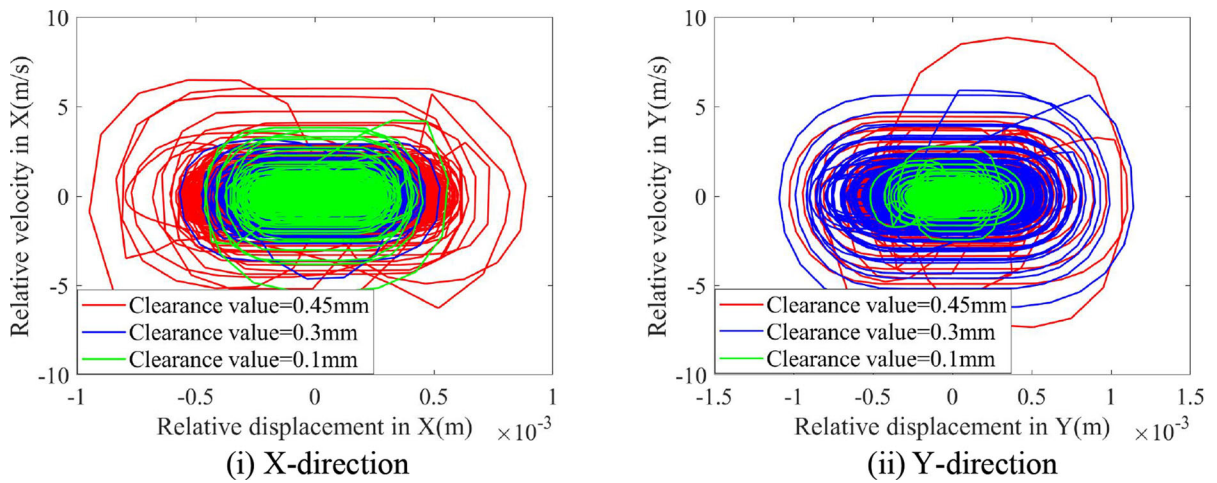
(i) X-direction

(ii) Y-direction

Fig. 31 Phase diagram of clearance A
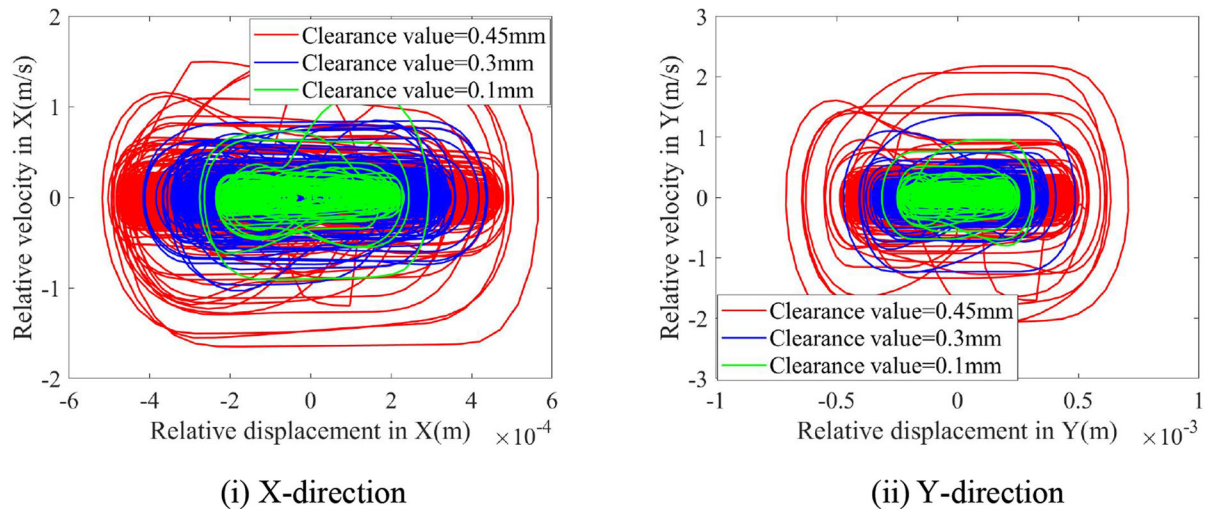

(i) X-direction

(ii) Y-direction

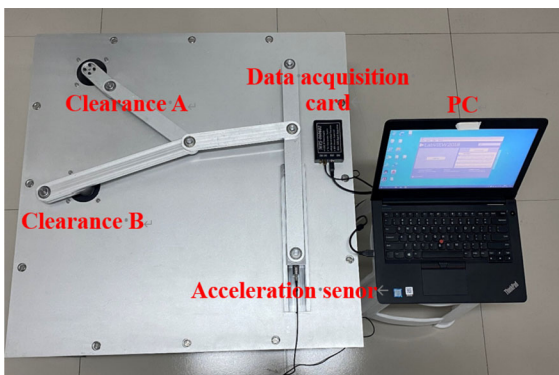**Fig. 32** Phase diagram of clearance B

Fig.33 Test bed of 9-bar mechanism

dynamics of mechanism is investigated, a test bed for 9-bar mechanism with clearances is designed to verify the correctness of the theoretical model. The main conclusions are:

1. The mathematical clearance model is constructed, where the normal contact force and tangential friction force of clearance are defined using the L-N model and the modified Coulomb friction model respectively. The dynamic model for 9-bar mechanism with uneven wear clearances is subsequently derived through the utilization of the Archard model and the Lagrange method.
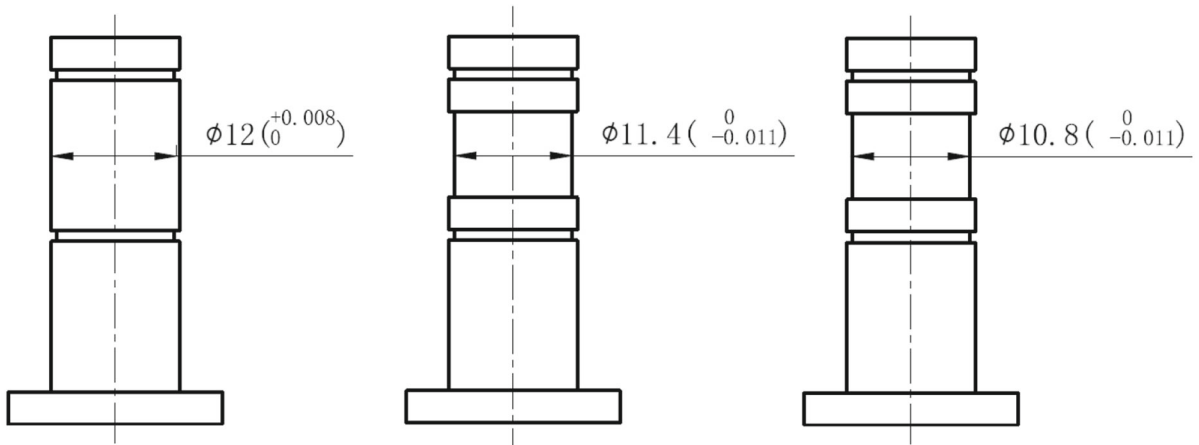
Fig. 34 CAD engineering drawing of clearance shaft
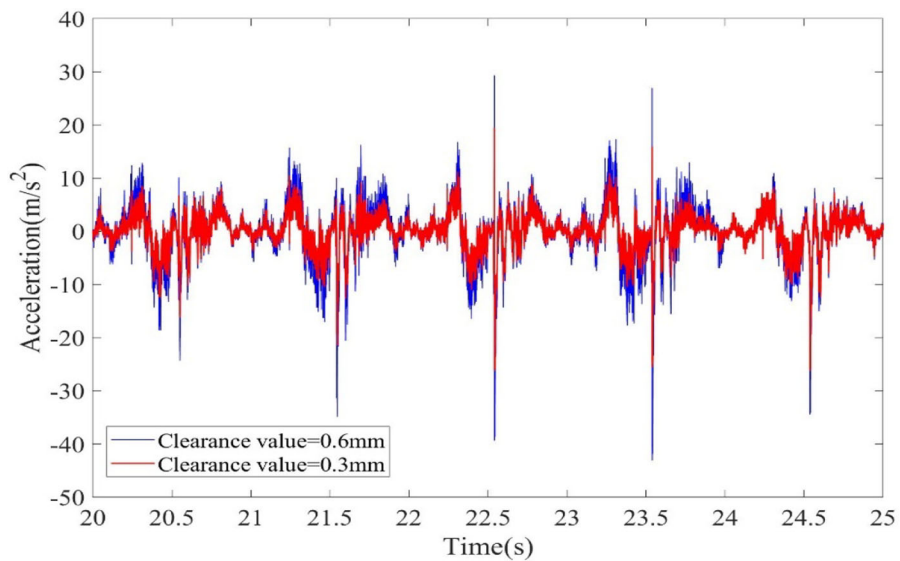

Fig. 35 Solid drawing of clearance shaft
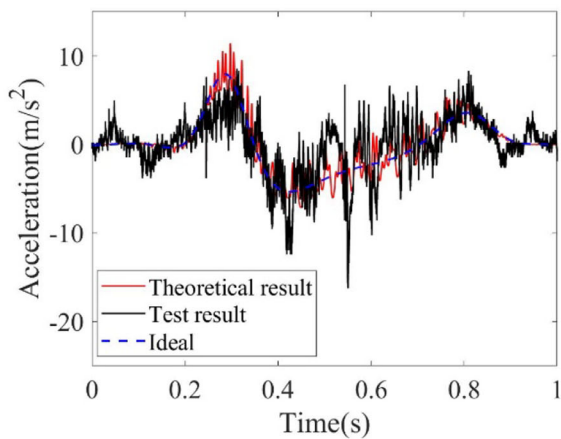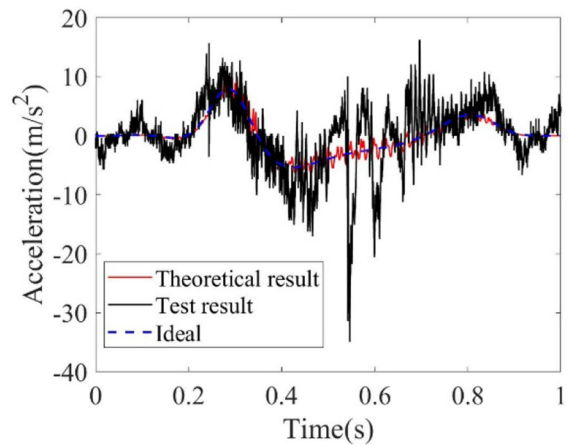

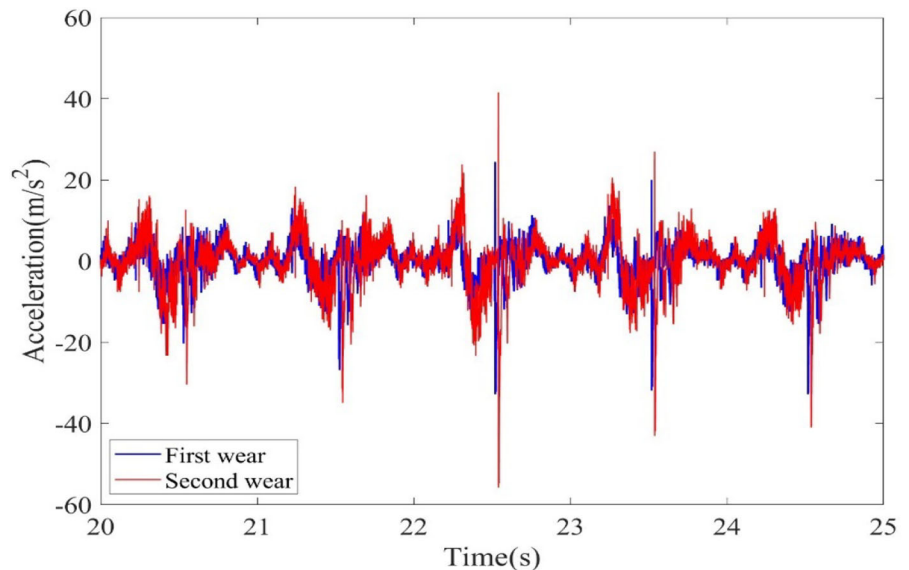**Fig. 36** Slider's acceleration

(i) Clearance value=0.3mm (ii) Clearance value=0.6mm

Fig. 37 Comparison of results

Fig. 38 Slider's acceleration

2. The effects of wear times and different initial clearance values on dynamic characteristics and nonlinear dynamics of 9-bar mechanism with uneven wear clearances are discussed. The results indicate that the wear clearances have a great influence on dynamic characteristics of mechanism. Second wear has a greater impact on mechanism than first wear, and the wear degree will increase positively with the increase of initial clearance values. In addition, through the analysis of nonlinear dynamics, it is found that clearance A and B are transforming from periodic motion to chaotic motion after wear.

3. The test bed of 9-bar mechanism is built, and the dynamic characteristics of the test bed under different clearance values before and after wear are compared with the theoretical results, respectively. The findings indicate a substantial
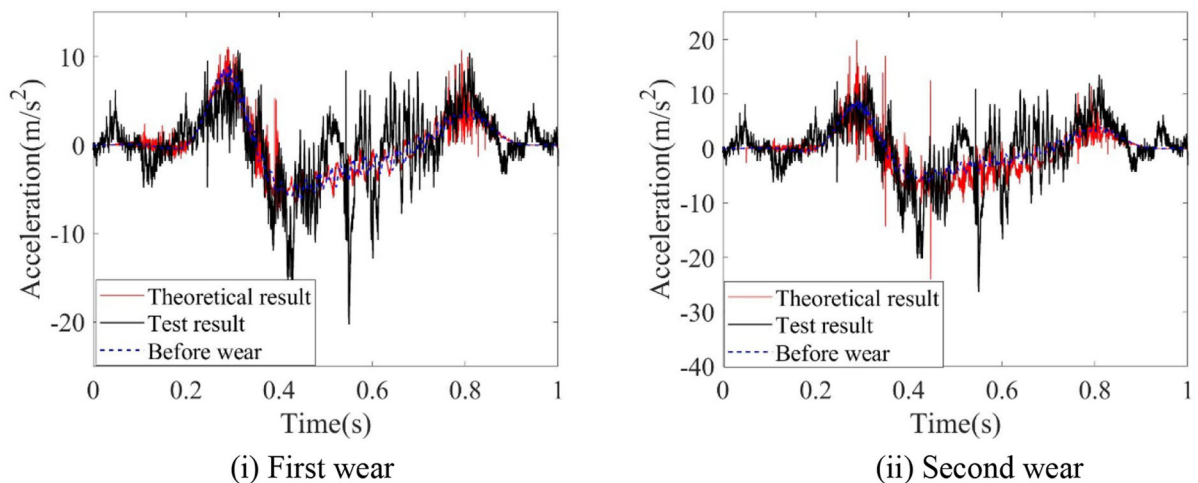
(i) First wear

(ii) Second wear

Fig. 39 Comparison of results

alignment between the experimental and theoretical data, thus confirming the validity and accuracy of the theoretical framework.

Declarations

Conflict of interest The authors declare that they have no conflict of interest.

References

1. Hu, F., Sun, Y., Peng, B.: Elastic dynamic research of high-speed multi-link precision press considering structural stiffness of rotation joints. J. Mech. Sci. Technol. **30**(10), 4657–4667 (2016)
2. Cao, L., Liu, J., Zhang, J., et al.: Positioning accuracy reliability analysis of industrial robots considering epistemic uncertainty and correlation. J. Mech. Des. **145**(2), 023303 (2023)
3. Pradhan, D., Ganguly, K., Swain, B., et al.: Optimal kinematic synthesis of 6 bar rack and pinion Ackerman steering linkage. Proc. Inst. Mech. Eng. D J. Automob. Eng. **235**(6), 1660–1669 (2021)
4. Earlcs, S.W.E., Wu, C.L.S.: Motion analysis of a rigid-link mechanism with clearance at a bearing, using Lagrangian mechanics and digital computation. In: Mechanisms (Proceedings, Institution of Mechanical Engineers), London, pp. 83–89 (1973)
5. Dubowsky, S., Freudenstein, F.: Dynamic analysis of mechanical systems with clearances—part 1: formation of dynamic model. J. Eng. Ind. **93**(1), 305–309 (1971)
6. Dubowsky, S., Freudenstein, F.: Dynamic analysis of mechanical systems with clearances—part 2: dynamic response. J. Eng. Ind. **93**(1), 310–316 (1971)
7. Miedema, B., Mansour, W.M.: Mechanical joints with clearance: a three-mode model. J. Eng. Ind. **98**(4), 1319–1323 (1976)
8. Soong, K., Thompson, B.S.: A theoretical and experimental investigation of the dynamic response of a slide-crank mechanism with radial clearance of the gudgeon-pin joint. J. Mech. Des. **112**(2), 183–189 (1990)
9. Ghayesh, M.H.: Dynamics of functionally graded viscoelastic microbeams. Int. J. Eng. Sci. **124**, 115–131 (2018)
10. Reis, V.L., Daniel, G.B., Cavalca, K.L.: Dynamic analysis of a lubricated planar slider-crank mechanism considering friction and Hertz contact effects. Mech. Mach. Theory **74**(6), 257–273 (2014)
11. Tan, X., Chen, G., Shao, H.: Modeling and analysis of spatial flexible mechanical systems with a spherical clearance joint based on the luGre friction model. J. Comput. Nonlinear Dyn. **15**(1), 011005 (2019)
12. Zhuang, X.: Time-dependent kinematic reliability of a dual-axis driving mechanism for satellite antenna considering non-uniform planar revolute joint clearance. Acta Astronaut. **197**, 91–106 (2022)
13. Tian, Q., Flores, P., Lankarani, H.M.: A comprehensive survey of the analytical, numerical and experimental methodologies for dynamics of multibody mechanical systems with clearance or imperfect joints. Mech. Mach. Theory **122**, 1–57 (2018)
14. Chen, Y., Feng, J., He, Q., et al.: A methodology for dynamic behavior analysis of the slider-crank mechanism

considering clearance joint. Int. J. Nonlinear Sci. Numer. Simul. **22**(3–4), 373–390 (2021)

15. Li, P., Chen, W., Li, D., et al.: Wear analysis of two revolute joints with clearance in multibody systems. J. Comput. Nonlinear Dyn. **11**(1), 011009 (2016)

16. Li, B., Wang, S., Gantes, C., et al.: Nonlinear dynamic characteristics and control of planar linear array deployable structures consisting of scissor-like elements with revolute clearance joint. Adv. Struct. Eng. **24**(7), 1439–1455 (2021)

17. Guo, J., Randall, R.B., Borghesani, P., et al.: A study on the effects of piston secondary motion in conjunction with clearance joints. Mech. Mach. Theory **149**, 103824 (2020)

18. Ordiz, M., Cuadrado, J., Cabello, M., et al.: Prediction of fatigue life in multibody systems considering the increase of dynamic loads due to wear in clearances. Mech. Mach. Theory **160**(5), 104293 (2021)

19. Wu, X., Sun, Y., Wang, Y., et al.: Dynamic analysis of the double crank mechanism with a 3D translational clearance joint employing a variable stiffness contact force model. Nonlinear Dyn. **99**(3), 1937–1958 (2020)

20. Zhuang, X., Yu, T., Shen, L., et al.: Time-varying dependence research on wear of revolute joints and reliability evaluation of a lock mechanism. Eng. Fail. Anal. **96**, 543–561 (2019)

21. Mukras, S., Kim, N., Mauntler, N., et al.: Analysis of planar multibody systems with revolute joint wear. Wear **268**(5–6), 643–652 (2010)

22. Alves, D.S., Fieux, G., Machado, T.H., et al.: A parametric model to identify hydrodynamic bearing wear at a single rotating speed. Tribol. Int. **153**, 106640 (2021)

23. Flores, P.: Modeling and simulation of wear in revolute clearance joints in multibody systems. Mech. Mach. Theory **44**(6), 1211–1222 (2009)

24. Singh, A., Sharma, S.C.: Analysis of a double layer porous hybrid journal bearing considering the combined influence of wear and non-Newtonian behaviour of lubricant. Meccanica **56**(1), 73–98 (2021)

25. Lai, X., He, H., Lai, Q., et al.: Computational prediction and experimental validation of revolute joint clearance wear in the low-velocity planar mechanism. Mech. Syst. Signal Process. **85**, 963–976 (2017)

26. Chen, X., Tang, Y., Gao, S.: Dynamic modeling and analysis of hybrid driven multi-link press mechanism considering non-uniform wear clearance of revolute joints. Meccanica **57**(1), 229–250 (2022)

27. Jiang, S., Chen, X.: Test study and nonlinear dynamic analysis of planar multi-link mechanism with compound clearances. Eur. J. Mech. A. Solids **88**(2), 104260 (2021)

28. Zhu, A., He, S., Zou, C., et al.: The effect analysis of contact stiffness on wear of clearance joint. J. Tribol. Trans. ASME **139**(3), 031403 (2017)

29. Zhuang, X., Yu, T., Liu, J., et al.: Kinematic reliability evaluation of high-precision planar mechanisms experiencing non-uniform wear in revolute joints. Mech. Syst. Signal Process. **169**, 108748 (2022)

30. Li, B., Wang, M., Gantes, C., et al.: Modeling and simulation for wear prediction in planar mechanical systems with multiple clearance joints. Nonlinear Dyn. **108**(2), 887–910 (2022)

31. Xiang, W., Yan, S.: Dynamic analysis of space robot manipulator considering clearance joint and parameter uncertainty: Modeling, analysis and quantification. Acta Astronaut. **169**, 158–169 (2020)

32. Erkaya, S., Uzmay, I.: Experimental investigation of joint clearance effects on the dynamics of a slider-crank mechanism. Multibody Syst. Dyn. **24**(1), 81–102 (2010)

33. Akhadkar, N., Acary, V., Brogliato, B.: Multibody systems with 3D revolute joints with clearances: an industrial case study with an experimental validation. Multibody Syst. Dyn. **42**(3), 249–282 (2018)

34. Flores, P., Koshy, C.S., Lankarani, H.M., et al.: Numerical and experimental investigation on multibody systems with revolute clearance joints. Nonlinear Dyn. **65**(4), 383–398 (2011)

35. Erkaya, S., Dogan, S., Ulus, S.: Effects of joint clearance on the dynamics of a partly compliant mechanism: numerical and experimental studies. Mech. Mach. Theory **88**, 125–140 (2015)

36. Zheng, E., Zhu, R., Zhu, S., et al.: A study on dynamics of flexible multi-link mechanism including joints with clearance and lubrication for ultra-precision presses. Nonlinear Dyn. **83**(1–2), 137–159 (2016)

37. Chen, X., Gao, S.: Dynamic response and dynamic accuracy reliability of planar mechanism with multiple lubricated clearances. Multibody Syst. Dyn. **57**, 1–23 (2022)

38. Chen, X., Gao, S.: Dynamic accuracy reliability modeling and analysis of planar multi-link mechanism with revolute clearances. Eur. J. Mech. A/Solids **90**, 104317 (2021)